Postprint of: Makarova I., Dobryden I., Kharitonov D., Kasach A., Ryl J., Repo E., Vuorinen E., Nickel-nanodiamond coatings electrodeposited from tartrate electrolyte at ambient temperature, Surface and Coatings Technology, Vol. 380 (2019), 125063, DOI: 10.1016/j.surfcoat.2019.125063

Nickel-nanodiamond coatings electrodeposited from tartrate electrolyte at ambient temperature

Irina Makarova [a, b,*], *Illia Dobryden* [c], *Dmitry Kharitonov* [a, d], *Aliaksandr Kasach* [a], *Jacek Ryl* [e], *Eveliina Repo* [b] *and Esa Vuorinen* [f]

[a] *Chemical Technology and Engineering Faculty, Department of Chemistry, Technology of Electrochemical Production and Electronic Engineering Materials, Belarusian State Technological University, Sverdlova str. 13a, 220006, Minsk, Republic of Belarus*

[b] *Department of Separation and Purification, School of Engineering Science, Lappeenranta University of Technology, Skinnarilankatu 34, FI-53850, Finland*

[c] *KTH Royal Institute of Technology, Surface and Corrosion Science Division, School of Engineering Sciences in Chemistry, Biotechnology and Health (CBH), Drottning Kristinas väg 51, SE-100 44 Stockholm, Sweden*

[d] *Jerzy Haber Institute of Catalysis and Surface Chemistry of Polish Academy of Sciences, 30-239, Niezapominajek 8, Krakow, Poland*

[e] *Gdansk University of Technology, Department of Electrochemistry, Corrosion and Materials Engineering, Narutowicza str. 11/12 , 80-233 Gdansk, Poland*

[f] *Luleå University of Technology, Department of Engineering Sciences and Mathematics, Regnbågsallén, 97187 Luleå, Sweden*

Abstract

Electrodeposition of composite electrochemical coatings is a good way to modify surface electrochemical and physicochemical properties. In this study, nanocrystalline Ni-ultradispersed diamond nanoparticles coatings were obtained by electrodeposition from a low-temperature tartrate electrolyte to achieve good material corrosion and wear protection. The following studies on microhardness, adhesion, wear and corrosion resistance were performed using atomic force microscopy, scanning electron microscopy, electrochemical impedance spectroscopy and linear polarization and demonstrated improved surface properties. The introduction of ultrafine diamond nanoparticles into the coating led to a rougher surface structure and a smaller grain size compared to bare nickel coating. This contributed to a clear increase in microhardness and wear resistance. The addition of such nanoparticles slightly improved the corrosion resistance of the coating and led to a decrease in corrosion current density and nobler values of the corrosion potential.

Keywords: electrolitic co-deposition; Ni-nanodiamond composite coating; kinetics; morphology; corrosion; wear

1. Introduction

Electrodeposition of composite electrochemical coatings (CECs) is a cheap and reliable way of surface modification to achieve desired properties, such as wear and corrosion resistance, abrasion resistance, and catalytic activity. Introduction of ultradispersed diamond nanoparticles (UDD) allows forming of fine-grained, densed, and low-porous coatings with improved hardness properties up to 2−5 times [1]. Moreover, such CEC materials with increased hardness can potentially be used in production of cutting tools [2]. A good metallic matrix needs to possess

* Corresponding author
E-mail: Iryna.Makarava@lut.fi

good adhesion to the substrate, a high degree of growth of the second (inert) phase, and the possibility of thick coating deposition to produce such CEC. Thus, Ni [3−7, 8], Co [9], Zn [10], Cu [11, 12] and their alloys (Co−W [13], Ni−Co [4, 14], Ni−Mo [15], Cu−Sn [16]) are among good candidates for matrix materials.

There are several studies reporting successful co-deposition of nickel with a carbon-containing phase, in particular graphite [17], carbon nanotubes [18], fullerenes [19, 20], and diamonds [1, 21–25]. Several studies on such diamond-CEC composites were conducted under different conditions. In detail, nickel coatings containing diamonds of various sizes ranging from 4–6 nm [22, 23, 26], 10 nm [27, 28], 500 nm [24] to several microns were investigated. The content of diamond particles in the formed coatings ranged from tenths to several weight percent. Wang L. et al. [1] investigated co-deposition of nano-sized diamond particles from Watts electrolyte and showed no impact of UDDs on the crystal texture and structure of nanocrystalline Ni matrix and revealed unexpected poorer wear resistance as compared with pure Ni coatings. However, the UDD's amount was not varied and a large concentration of UDD (10 $g \cdot L^{-1}$) was used. Such a large concentration can potentially hinder any improving of nanomechanical properties. Thus, more studies are needed to investigate and elucidate UDDs concentration and composite preparation effect on its mechanical, tribological, and corrosion properties.

It was shown that the ultradispersed diamond nanoparticles are of a shape close to oval or spherical without sharp edges and possess a combination of unique properties, such as a large specific surface area (up to 450 m^2), high surface energy, and a complex structure. This structure is presented in Fig. 1*a*, as a sketch [29, 30] with the classical cubic diamond core (size of ~ 40 Å) and the carbon shell containing amorphous carbon structures (4–10 Å). This shell consists of sp^2 hybridized carbon atoms with oxygen-containing functional groups. The non-diamond components of pure UDDs are the part of the produced material, affecting the overall material properties [31].

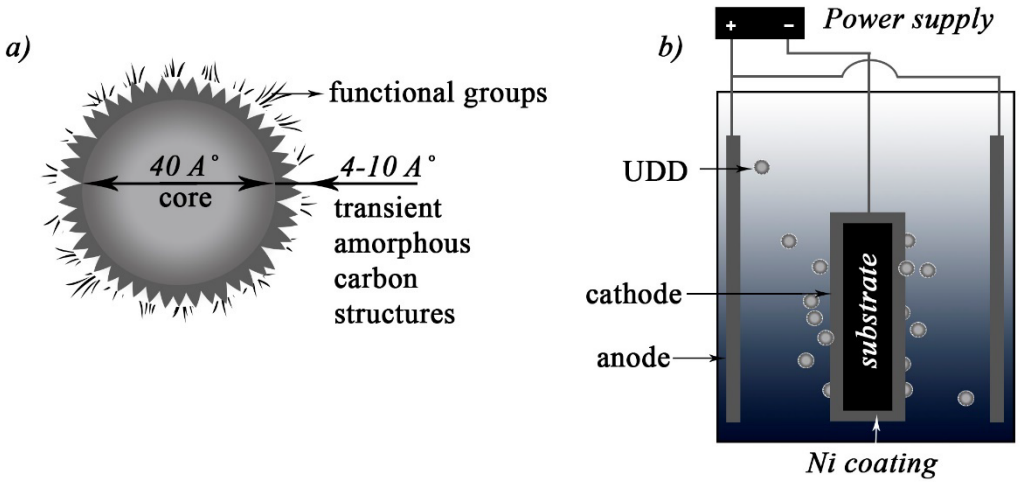

* Corresponding author
E-mail: Iryna.Makarava@lut.fi

Fig. 1. Schematic illustration of Ultra-dispersed diamonds (UDDs) structure (*a*) and their co-deposition during cathodic electrodeposition of metals; Scheme of the electrodeposition (*b*)

The size of the crystallites (grain) in the matrix have a large influence on the physico-mechanical properties of the result coating [11]. Nickel belongs to a group of metals allowing the formation of fine crystalline adhesive coatings [32–34]. Commonly used electrolyte for the electrodeposition of nickel coatings is a mixture of nickel sulfate and nickel chloride with the addition of boric acid as a buffer additive (Watts electrolyte) [35, 36]. The solution is operated at high temperatures (50–55 ºC), otherwise, it is impossible to achieve current efficiency close to 100% during deposition. The elevated temperature leads to fast evaporation of electrolyte, necessity of an additional time for electrolyte heating, and control of temperature during electrolysis [25]. In previous works [25, 37, 38], it was shown that replacing the buffer and complexing additive H_3BO_3 in nickel-plating electrolyte with organic components (acids and salts) allow the formation of Ni coatings with desired functional- and performance-properties at ambient temperatures. This work is a continuation of previous study [25] on the electrodeposition of Ni-based CEC from electrolytes at a low temperature with extension on mechanical, tribological, and corrosion properties of the UDDs containing coatings. In particular, the effect of UDD concentration on these properties and also on the composition and structure of the coatings have been studied.

2. Experimental

2.1. Sample preparation and coating electrodeposition

The electrodeposition of CEC nickel–UDD coatings was performed from a low-temperature tartaric bath. During the electrodeposition, carbon steel or copper plates were used as the cathode and a pure Ni plate was used as the anode. The analytical reagent grade chemicals were dissolved in distilled water to form the electrolytic solution. Cathodes were mechanically grinded with #1200 and #2000 emery paper and then suspended in a degreasing bath containing, (in $g \cdot dm^{-3}$): Na_2CO_3 − 30, $Na_3PO_4 \cdot 12H_2O$ − 30, NaOH − 40 at 60−80 ºC. Copper plates were additionally electrochemically treated cathodically in a degreasing bath, (in $g \cdot dm^{-3}$): Na_2CO_3 − 30, $Na_3PO_4 \cdot 12H_2O$ − 30 at 50−60 ºC for 1−2 min at a current density of 1 $kA \cdot m^{-2}$. After that, the sheets were chemically etched in 0.1 M sulfuric acid at ambient temperature in order to obtain the contamination-free surface.

The bath composition and its operating conditions are listed in Table 1. The schematic representation of the electrochemical electrodeposition of a composite coating is shown in Fig. 1, *b*. The Rochelle salt ($KNaC_4H_4O_6 \cdot 4H_2O$) concentration was 0.2 ($mol \cdot dm^{-3}$). In order to

* Corresponding author
E-mail: Iryna.Makarava@lut.fi

study the kinetic features of nickel oxidation and reduction in the presence of UDDs concentration of $KNaC_4H_4O_6 \cdot 4H_2O$ was varied from 0.05 to 0.3 ($mol \cdot dm^{-3}$) and Ni^{2+} from 0.7 to 1.0 ($mol \cdot dm^{-3}$). The suspension bath was stirred by a mechanical stirrer at a stable rotational speed (300 rpm). Ultradispersed diamonds with an average nominal diameter of 6 nm («SINTA», Belarus) obtained by denotational synthesis were used as the second phase. The temperature of solution during the electrolysis was controlled by a 5 OK-20/0,05-02 water thermostat (5 Okeanov, Belarus) in a beaker with a jacket. After the plating process, the deposits were washed with distilled water and dried with a flow of air.

Table 1. Bath composition and electrodeposition parameters

Component/parameter	Value
$NiSO_4 \cdot 7H_2O$	0.8 ($mol \cdot dm^{-3}$)
$NiCl_2 \cdot 6H_2O$	0.2 ($mol \cdot dm^{-3}$)
Rochelle Salt	0.1 ($mol \cdot dm^{-3}$)
Diamond Particles	$0–5 \cdot 10^{-2}$ ($g \cdot dm^{-3}$)
Stirring Rate	300 (rpm)
Current Density	2 ($A \cdot dm^{-2}$)
Temperature	20–25 ºC

2.2. Surface analysis

A scanning electron microscope (JEOL JSM–5610 LV) and a Nanosurf Flex-Axiom AFM system (Bruker, Germany) atomic force microscope were used to investigate the surface and cross-section morphology and topography. The AFM measurements were conducted in the tapping mode using a *n*-type silicon cantilever with a nominal tip radius of 15 nm (HQ:NSC15, MikroMasch). Chemical composition of the coatings was identified by an energy dispersive X-ray spectroscopy (EDS) system of the scanning electron microscope. The contact potential difference voltage (V_{CPD}) and phase mapping of reference nickel coating and coating containing 0.05 ($g \cdot dm^{-3}$) of UDDs (concentration in electrolyte) were performed with Intermodulation AFM (ImAFM) and Intermodulation Electrostatic Force Microscopy (ImEFM) on a Bruker Dimension Icon AFM (Bruker, USA) connected to a multi-frequency lock-in amplifier (Intermodulation Products AB, Sweden). More details on the ImAFM and ImEFM techniques can be found in [39, 40]. The data were analyzed using the IMP software suite (version 1.1, Intermodulation Products AB) and processed with Gwyddion software (version 2.44). The measurements were conducted using NCH-20 (with platinum coating) probes with a nominal spring constant of 42 N/m. The

* Corresponding author
E-mail: Iryna.Makarava@lut.fi

ImEFM measurements were taken at a 1 Hz acquisition speed and the measured areas contain 256×256 data points.

A D8 Advance AXS X-ray diffractometer (Bruker, Germany) with Cu *K*α radiation (λ= 1.5418 Å) was employed to obtain XRD spectra. The XRD spectra were analyzed by Match! software. The average grain diameter was calculated using the Scherrer equation, as follows:

$$d = \frac{0,9 \cdot \lambda}{b \cdot \cos\theta}, \tag{1}$$

where b is the FWHM, θ is the diffraction angle, d is the grain size, and λ (0.15405 nm) is the wavelength of the radiation used.

2.2. Mechanical and tribological studies

The microhardness of the obtained coatings was tested by a Vickers hardness indenter (Matsuzawa MXT-CX) with a load of 100 g for 15 s. Each microhardness value was calculated as an average of ten measurements.

The coating wear resistance was examined under the dry sliding condition in air at 25 C for 30 min by the pin-on-disk method. All wear tests were performed against 7 mm diameter ruby balls under the load of 1 N at a fixed rotation speed of 200 rpm. For each type of the samples, three tests were carried out under the same conditions. After the wear test, worn surface morphology was evaluated using optical microscopy.

2.3. Electrochemical measurements

Electrochemical measurements were carried out in a three-electrode cell with saturated silver/silver-chloride electrode as a reference electrode, platinum wire as a counter electrode, and nickel or a copper substrate with electrodeposited nickel–UDD coating (exposed surface area 1 cm^2) as a working electrode using an Autolab PGSTAT 302N potentiostat-galvanostat (Methrom Autolab, The Netherlands). In order to study influence of UDD on kinetic process of deposition and oxidation diamond particles were added to electrochemical set-up. Prior to experiments, working electrodes were immersed in the electrolyte for 30 min with the moment of immersion as zero. Cathodic and anodic polarization was carried out potentiodynamically at a 5 $mV \cdot s^{-1}$ sweep rate. The temperature was controlled by a water jacket using a liquid thermostat. The solution pH was adjusted to 2 using 0.1 M H_2SO_4.

From the linear polarization curves of nickel electrode common kinetic parameters of oxidation and reduction process were determined. The OCP potentials were recorded 5 minutes after adjustment of the current at increasing and decreasing current densities until reproducible values were achieved. By linear fitting of Tafel curves η−lg i (eq. 2), the Tafel slope (b) (eq. 3), of the curve was obtained.

* Corresponding author
E-mail: Iryna.Makarava@lut.fi

$$\eta = -\frac{2{,}303RT}{\alpha nF} lgi_0 - \frac{2{,}303RT}{\alpha nF} lgi = a + blgi, \quad (2)$$

$$b = -\frac{2{,}303RT}{\alpha nF}, \quad (3)$$

where η is the overpotential (V), b is the Tafel slope (V decade^{-1}), α is the transfer coefficient, and i is the current density (A cm^{-2}). The exchange current densities i_o for nickel deposition were found by extrapolating the Tafel regions to zero overpotential

According to Tafel formula (eq. 2) the equation $lgi_0 = \frac{a}{b}$ can be deducted. The charge transfer coefficient (α) was calculated using the following equation $\alpha = -\frac{2{,}303RT}{bnF}$.

To determine susceptibility of obtained Ni and Ni-UDD coatings to localized corrosion in aqueous 0.5 M NaCl solution (chloride environment) linear polarization measurements were performed at the room temperature at 1 mV·s^{-1} sweep rate according to ASTM G 61-86. Electrochemical impedance spectroscopy spectra (EIS) were recorded at OCP in an applied frequency ranged from 10 kHz down to 0.01 Hz with a wave amplitude of 10 mV. All measurements were performed at least triplicate at the room temperature.

3. Results and discussion

3.1 Kinetics of nickel electrodeposition and dissolution in the presence of UDDs

Fig. 2 shows the effect of the second phase (UDD) introduction on the cathodic (Fig. 2, *a*) and anodic (Fig. 2, *b*) polarization of nickel electrode in tartrate electrolyte. This allows to characterize the kinetic features of nickel reduction and oxidation, respectively.

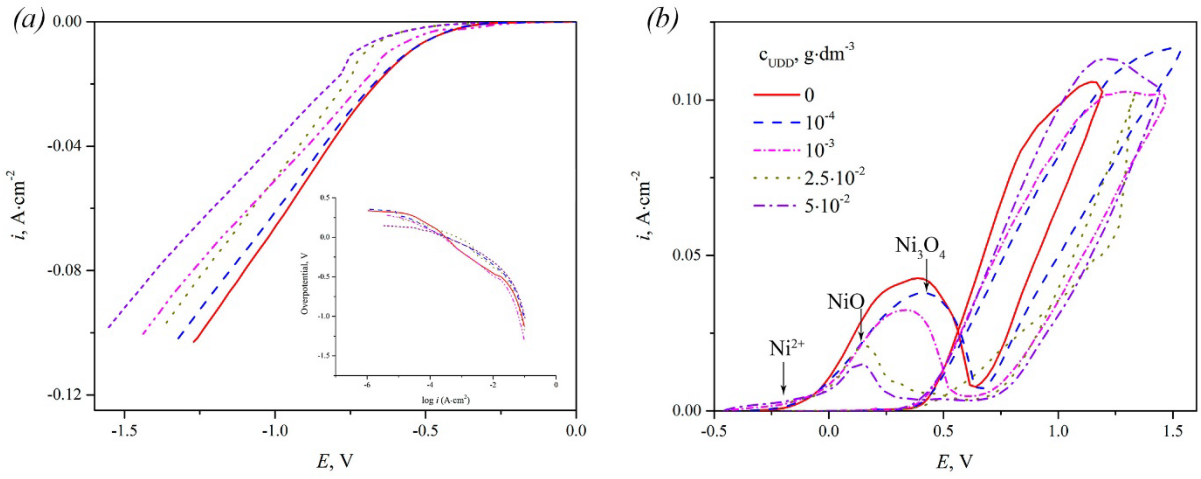

Fig. 2. Cathodic (*a*) and anodic (*b*) polarization curves of nickel electrode in the presence of UDDs (potentials vs SHE). Inset plot in (a) shows Tafel partial cathodic polarization curves of nickel electrode

* Corresponding author
E-mail: Iryna.Makarava@lut.fi

The OCP (Fig. 2, *a*) remained almost unchanged with UDDs addition in electrolyte. With the other hand, the presence of UDD particles leads to an increase in cathodic polarization. This is probably due to the adsorption of nanodiamonds on the surface of the cathode that impedes the reduction of nickel ions with a decrease in active surface area of cathode [18] and was observed in similar systems [10].

The main kinetic parameters of the nickel electrode were calculated from the linear polarization curves (Fig. 2) and are presented in Table 2. The abscissa of the each polarization curve in Fig. 2 is subtracted from the respective OCP, then multiplied by −1, and transformed to the overpotential. On the basis of the above, the ordinate of each curve is divided by the electrode area and multiplied on current efficiency, and their logarithms was taken. The resulting partial cathodic Tafel curves of Ni electrodeposition at different concentrations of UDD nanoparticles are presented as the inset in Fig.2, *a*.

Table 2 Kinetic parameters of nickel reduction and oxidation in tartaric electrolyte with UDDs addition

C_{UDD}, g·dm^{-3}	Cathodic branch (±0,005 V)		Anodic branch (±0,005 V)		$\alpha_к$	i_o, A·m^{-2}
	a, V	|*b*|·dec, V	*a*, V	*b*·dec, V		
0	−0.495	0.145	1.445	0.506	0.03	$1.78\cdot10^{-2}$
$1\cdot10^{-4}$	−0.220	0.137	0.655	0.259	0.22	$2.83\cdot10^{-2}$
$1\cdot10^{-3}$	−0.187	0.131	0.626	0.277	0.23	$3.18\cdot10^{-2}$
$2{,}5\cdot10^{-2}$	−0.257	0.136	0.330	0.159	0.05	$2.11\cdot10^{-2}$
$5\cdot10^{-2}$	−0.178	0.132	0.405	0.231	0.22	$4.20\cdot10^{-2}$

Coefficient *b* during the reduction of nickel was between –0.13 and –0.14 V both in the electrolyte with and without the UDD addition, testifying the invariance of the electroplating process and corresponding that the attachment of the first electron is the limiting stage of the process [41]. Thus, the limiting stage of nickel ion reduction in the potential range from –0.4 to –0.8 V is the electron transfer stage and, therefore, the addition of UDDs does not change the Ni^{2+} reduction mechanism, which can be shown as following steps:

$$Ni^{2+} + e^- \rightarrow Ni^+ \text{ (limiting stage)} \quad (4)$$

$$Ni^+ + e^- \rightarrow Ni \quad (5)$$

The current density of electrodeposition of nickel increases from $1.78\cdot10^{-2}$ to $4.20\cdot10^{-2}$ A·m^{-2} with an increase of UDD concentration in electrolyte from 0 to $5\cdot10^{-2}$ g·dm^{-3}. The exchange current density i_0 is usually increased when the electrochemical reaction is

* Corresponding author
E-mail: Iryna.Makarava@lut.fi

accelerated [42]. This increase of reaction speed implies that UDD nanoparticles accelerate the rate of Ni^{2+} ion transfer across the electrical double layer. The accelerating effect of UDDs could be due to their adsorption capability [43] on cathode and changing of the surface area.

The beginning of the nickel oxidation process (Fig. 2, *b*, eq. 6) is observed at more noble potentials than (–0.25) V, besides, there is one oxidation peak in the potential range of 0.2–0.6 V. Also, there is a tendency of the oxidation peak to shift to the region of more electronegative values with an increase of UDD concentration from 0 to $5 \cdot 10^{-2}$ g·dm^{-3}. This shift indicates the possibility of the occurrence of processes described in eq. (7) and eq. (8) and also can indicate a possible change in the form of nickel oxide being formed. It can be expected that Ni_3O_4 is forming due to the blocking of the electrode surface during adsorption of UDDs and the local decrease in i_{peak} [41].

$$Ni \rightarrow Ni^{2+} + 2e^- \qquad E° = -0.250 \text{ V} \quad (6)$$

$$Ni + H_2O = NiO + 2H^+ + 2e^- \qquad E° = 0.11 \text{ V} \quad (7)$$

$$3Ni + 4H_2O = Ni_3O_4 + 8H^+ + 8e^- \qquad E° = 0.307 \text{ V} \quad (8)$$

3.2 Structure characteristics and properties of nickel and nickel-UDD coatings

Diffractograms of nickel and nickel-UDD coatings for 2θ ranging 40–55° are presented in Fig. 3.

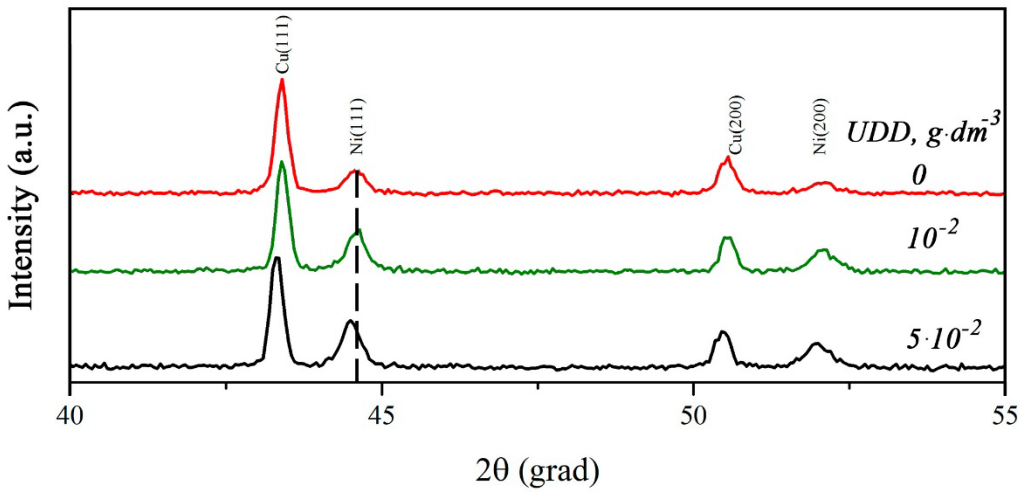

Fig. 3. XRD patterns of nickel and nickel-UDD coatings (concentration of UDD in the electrolyte is indicated).

* Corresponding author
E-mail: Iryna.Makarava@lut.fi

The peaks corresponding to copper and nickel were detected in the presented diffractograms. These peaks represent the data measured for the Cu substrate and the Ni coating. There is a tendency for the diffraction peaks broadening approximately about 20% for both Ni and Cu at (111) and (200) with an increase in the UDD content to 0.05 g·dm^{-3}. A peak of higher intensity for the nickel at about 44.5 degrees corresponds to (111) plane and at 52.2 degrees corresponds to the (200) plane. Both peaks are sensitive to the addition of UDDs and broadening also validates the change in UDDs concentration in the coatings. It can be concluded that UDD nanoparticles modify the structure of Ni matrix [15]. Similar results were also found in other systems [3, 18]. The absence of UDD diffraction peaks is due to the low (<5%) concentration which is below the detection limit. Note that the EDS analysis revealed peak at 0.3 keV, which can be associated with carbon based (UDDs) species in the coating (as shown in the supplementary Fig. S1).

The UDD addition influences the size of the nickel crystal in the formed coating. Increasing of UDD concentration in the electrolyte from 0 to 0.05 g·dm^{-3} is accompanied by a slight increase in the size of Ni crystals from 16.3 to 22.5 nm, as estimated using the Scherrer equation (1). The Ni crystalline size dependence on the UDD concentration can be associated with the different rates of metal nucleus grow during the coating electrodeposition. The UDD particles are uniformly distributed in the solution and are adsorbed on the growing nickel matrix and slightly increase crystal growth, thus decreasing nucleation [44].

3.3 Surface characteristics of nickel and nickel-UDD coatings

Morphology of the coating surfaces has changed with addition of UDDs as shown in SEM images (Fig. 4). Electrodeposition of nickel and CEC with UDDs at the concentration of 0.001 g·dm^{-3} in the electrolyte allowed to obtain uniform fine-crystalline coating with the crystal sizes of about 0.1–0.2 μm. The increase of UDD concentration to 0.05 g·dm^{-3} led to the coarsening of particles and formation of the structures of about 0.4–0.7 μm in size.

* Corresponding author
E-mail: Iryna.Makarava@lut.fi

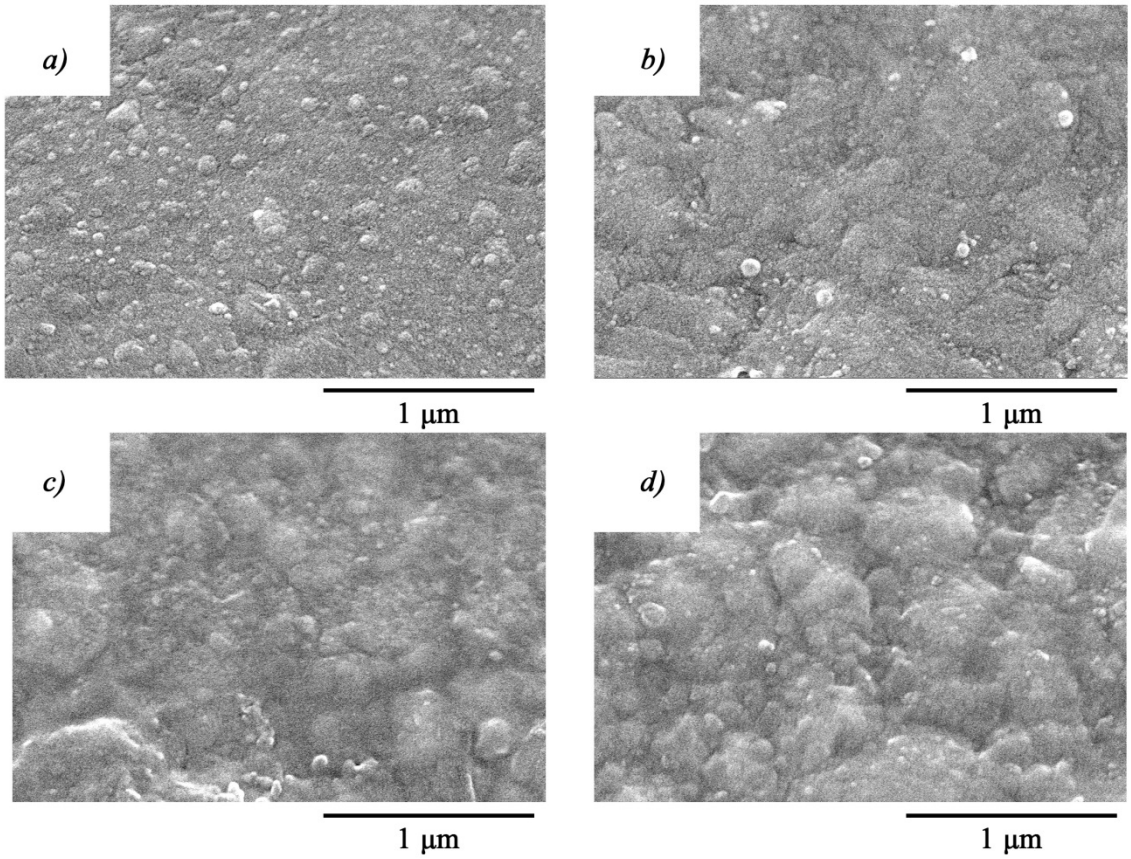

Concentration of UDD in electrolyte, g·dm^{-3}: *a* – 0, *b* – 0.001; *c* – 0.01; *d* – 0.05

Fig. 4. Microstructure of Ni (*a*) and Ni-UDD (*b*-*d*) coatings

The presence of 0.05 g·dm^{-3} UDD (Fig. 4, *d*) in the electrolyte caused significant agglomeration of the nanodiamonds (up to 2–5 μm) and it was also observed in our previous work [25].

The cross sections of pure Ni and Ni-UDD coatings are shown in Fig. 5.

* Corresponding author
E-mail: Iryna.Makarava@lut.fi

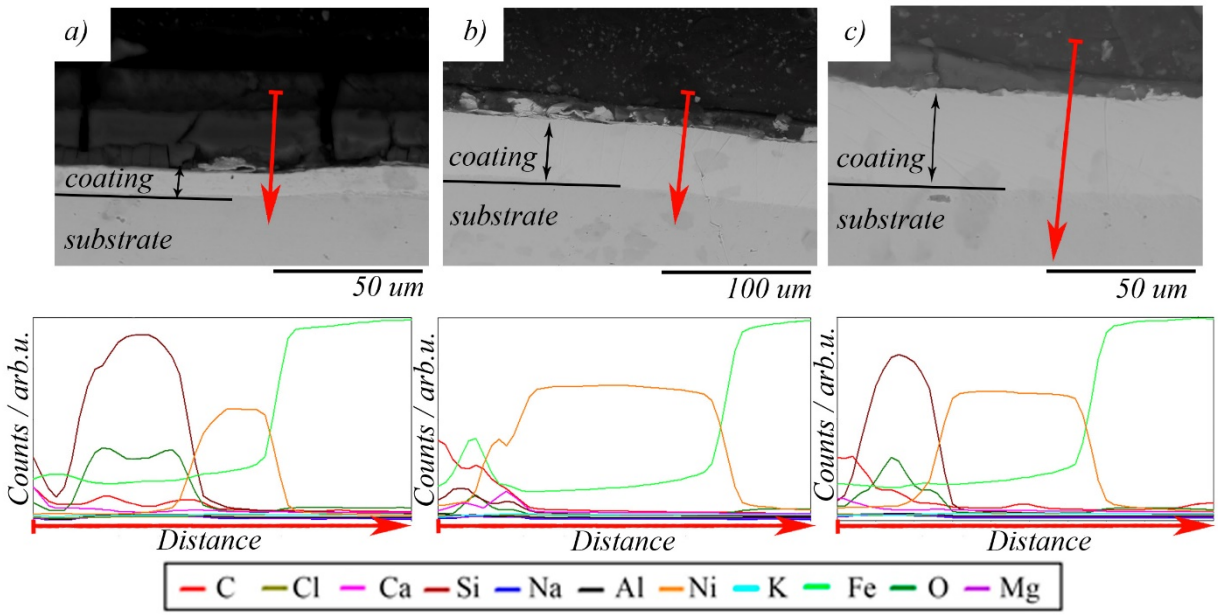

UDD in electrolyte, g·dm^{-3}: *a* – 0; *b* – 0.01; *c* – 0.05

Fig. 5. Microphotographs of cross-sections and corresponding elemental distribution (red arrow shows place and direction of the scan)

Ni and Ni-UDD coatings have homogenies distribution with clear lines between the substrate and coating which can suggest a good adhesion. The good adhesion between the coating and substrate is demonstrated later in adhesion measurements (Table 6).

The obtained coatings were examined for the surface robustness via the wear tests. The results of wear tests in dry conditions are shown in Fig. 6.

* Corresponding author
E-mail: Iryna.Makarava@lut.fi

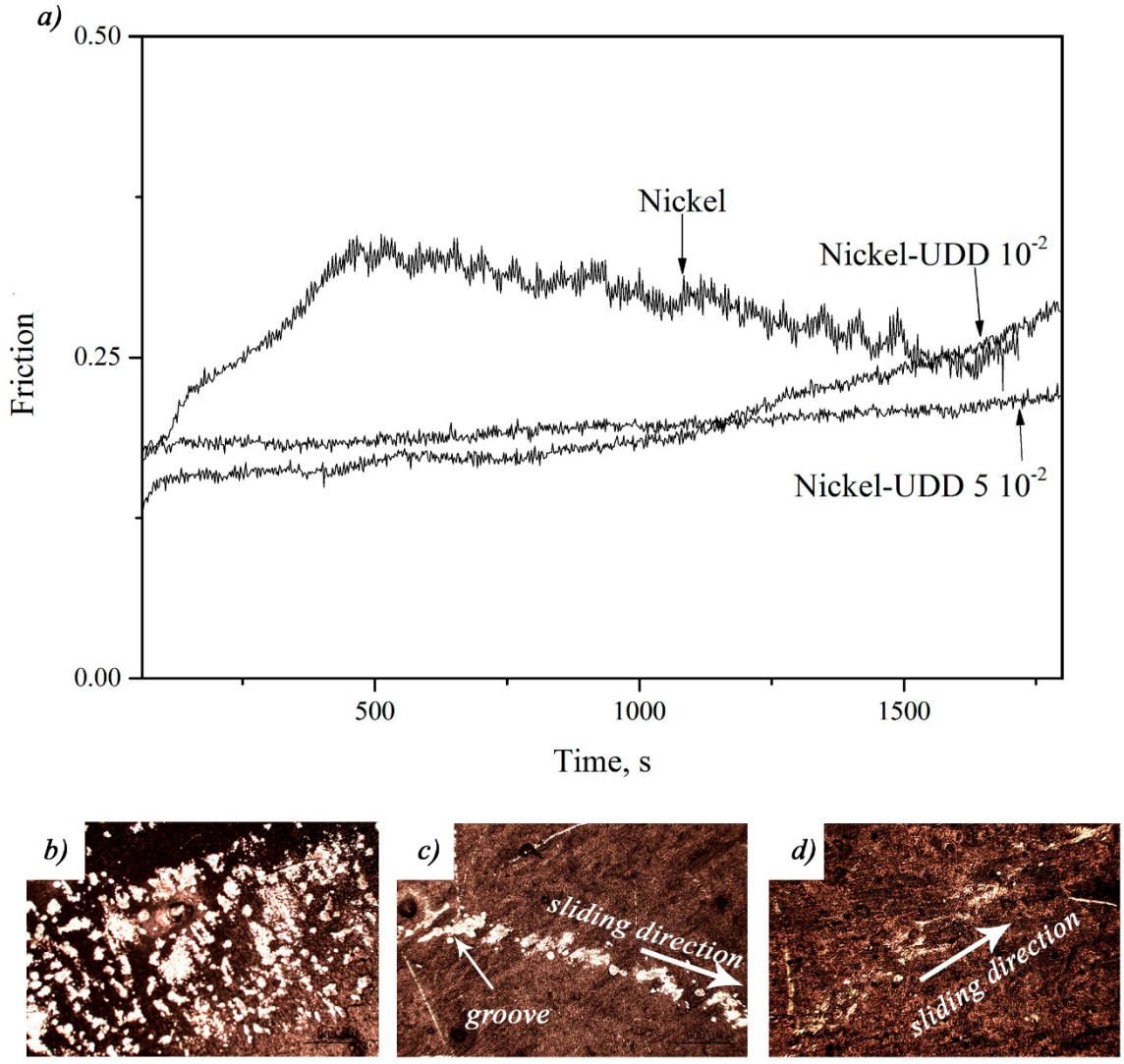

UDD concentration in electrolyte, g·dm^{-3}: *a* – 0; *b* – 10^{-2}; *c* – $5 \cdot 10^{-2}$

Fig. 6. Wear rate of nickel and nickel-UDD composite coatings (*a*) and optical micrographs of wear scars (*b–d*)

A lower wear rate is observed for the UDD-containing coatings as compared with the bare nickel coating that connected with forming of less-uniform sediment (Fig.4, *c*, *d*) with bigger crystals (Fig. 3). At the initial stage of testing (run-in stage), the friction coefficient of pure nickel coating is about 0.18. The friction has gradually increased to 0.33–0.34 after 400 s with a slight decrease to 0.28–0.30 after 500 s. The friction coefficient for the UDD contained nickel coatings remained almost constant up to about 1000 s following with a slight increase up to 0.20. This increase of the friction at the later stage (ca. 1500 s) is possibly due to occurrence of the abrasive wear. The measured friction was lower for the UDD-containing coatings than for the pure Ni coating. Thus, former have better tribological properties and addition of

* Corresponding author
E-mail: Iryna.Makarava@lut.fi

nanodiamonds can have a lubricating effect. Optical micrographs of wear scars reveal clear smooth traces of wear machine. Groove of sliding is less visible for the UDD-containing coatings (Fig. 6, *d*).

The roughness of the initial Ni coating and Ni coating containing $5 \cdot 10^{-2}$ UDDs was evaluated with AFM. The measured topography maps with the corresponding roughness cross-sections are shown in Fig. 7. There is some tendency for the roughness increase of the UDD-containing coatings in compare with the pure coating due to possible UDD agglomeration in the electrolyte as previously reported in [12].

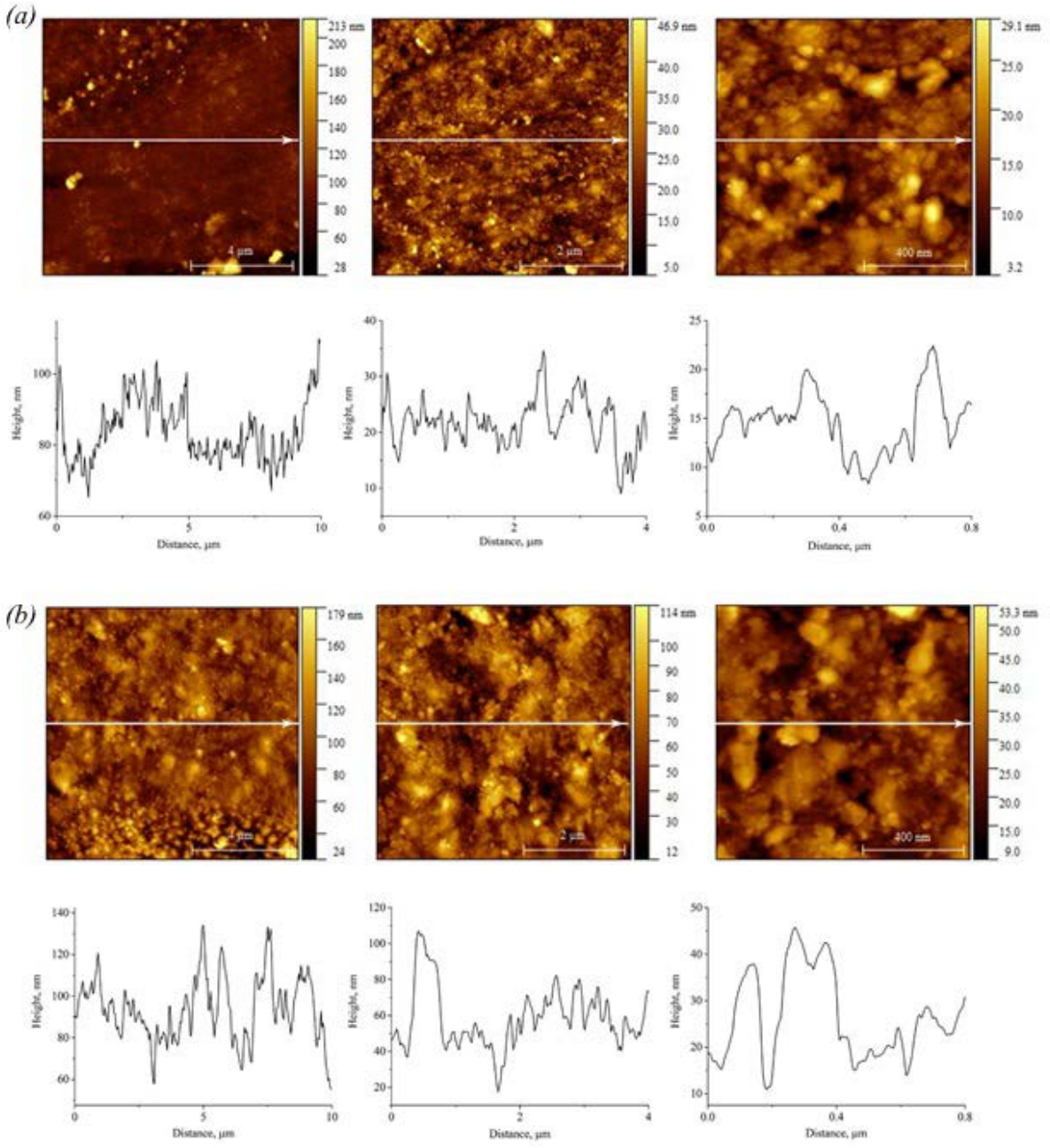

UDD in electrolyte, $g \cdot dm^{-3}$: *a* – 0; *b* – $5 \cdot 10^{-2}$

Fig. 7. AFM topography images of nickel (*a*) and nickel-UDD (*b*)coatings and corresponding roughness profiles along the lines indicated in the AFM images.

* Corresponding author
E-mail: Iryna.Makarava@lut.fi

The average roughness (R_a) was evaluated for all three studied areas and is presented in Table 6. Higher concentration of UDDs in the electrolyte leads to a higher roughness and microhardness of the coatings obtained as reported in Table 6.

Table 6. Properties of nickel and nickel-UDD coatings (UDD in electrolyte $5 \cdot 10^{-2}$ g·dm^{-3}).

		Nickel	Nickel-UDD
Roughness $R_{a,}$ nm	10×10 μm	3.04	7.27
	4×4 μm	2.71	7.55
	0.8×0.8 μm	1.14	3.23
Microhardness, HV	coating	198	306
	cross-section	280	450
Adhesion, MPa		>1.2 MPa	>1.2 MPa

Presence of 0.05 g·dm^{-3} UDD in the nickel-plating electrolyte contributes to a 1.5-times increase in the microhardness compared to the bare nickel coating. The microhardness of the cross-section reaches 450 HV and slightly changes along the length of the thin section, which indicates uniform distribution of the second phase over the matrix surface. This observation can be explained by surface texture changes of nickel and composite hardening due to addition of the UDDs [4]. The adhesion of nickel and CEC coatings to the substrate is similar and satisfactory. The coatings can withstand more than 1.2 MPa before they are detached from the substrate.

The ImEFM technique was applied to identify UDD nanoparticles or possible clusters in the nickel matrix, as shown in Fig. 8. To distinguish such small nanoparticles of 10 nm sizes in the matrix is a challenging task. Topographical images measured with AFM are often not sensitive to different material properties and thus such small nanoparticles will show no difference in contrast. With other hand, phase imaging in tapping mode and more advanced AFM methods such as PeakForce quantitative nanomechanical mapping (PeakForce QNM) can potentially be applied. However, elastic modulus of nickel metal is very high and would require to use an AFM cantilever with a very high spring constant and expensive diamond tip. Thus, a better option is to map these nanoparticles by differences in their surface potential, or measured V_{cpd}, with ImEFM offering high potential and lateral resolution. For the reference nickel coating containing no UDDs the phase (Fig 8, 1 *a* and 1 *b*) and surface potential images (Fig 8, 2 *a* and 2 *b*) measured in ImEFM do not show any clear nanoparticles. The areas with higher potential, but still in negative volts, as expected for nickel, are possibly related to higher nickel density or different surface oxide thickness. Also, these particle-like areas are of sizes larger than 100 nm.

* Corresponding author
E-mail: Iryna.Makarava@lut.fi

The corresponding topographical images (Fig 8, 3 *a* and 3 *b*) for the reference nickel coating demonstrate no clear topography since the measurement setpoint was optimized to minimize a possible cross-talk between surface topography and the measured potential. Mapping of UDD nanoparticles required to increase the measurement setpoint and scan the surfaces at high imaging force in case of nanocomposite containing 0.05 $g \cdot dm^{-3}$ UDDs in electrolyte. This was probably due to a presence of an oxide film on the surface hindering the nanoparticle potential. Clear small areas with a positive surface potential can be observed in the V_{cpd} images measured on the nanocomposite surface, as shown in Fig. 8 (2 *c* and 2 *d*). The figure 2, *d* is a repeat scan of the same location and highlights the same small areas. These areas are of sizes ranging in between 10−20 nm and can potentially be identified as UDDs nanoparticles. Also, the phase images measured simultaneously in ImAFM and sensitive to surface stiffness demonstrate different phase change for these small nanoparticles, as shown in Figure 8 (1 *c* and 1 *d*). This is an interesting result that ImAFM method can distinguish two such hard materials at nanoscale. The topography images for the nanocomposite are shown in Fig. 8 (3 *c* and 3 *d*). The surface features are well seen due to higher imaging force, which also leads to the unwanted cross-talk between topography and potential. Thus, these measurements should be considered more qualitative than quantitative with the main aim to visualize such small nanoparticles in this nanocomposite. This can be of importance for further studies.

* Corresponding author
E-mail: Iryna.Makarava@lut.fi

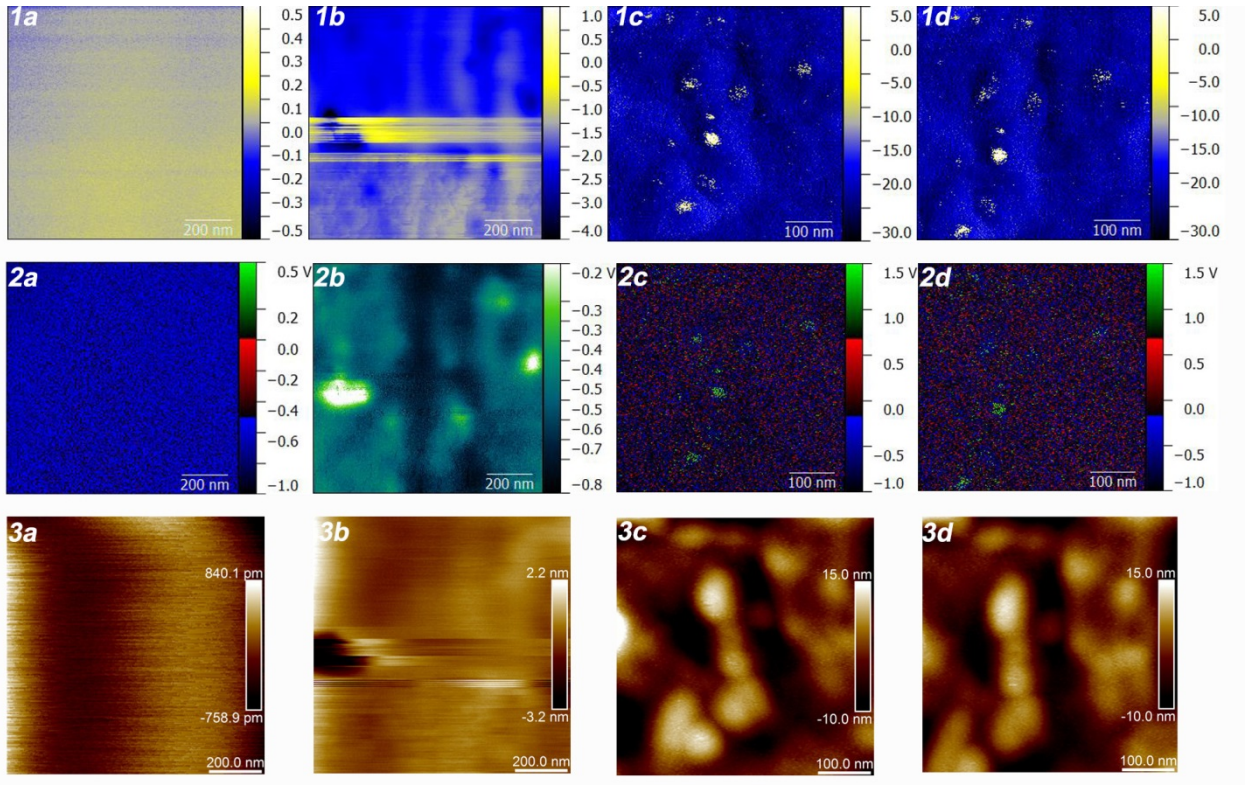

Fig. 8. The phase images measured in ImAFM for the reference nickel coating are in (1 *a*, *b*) and for the nanocomposite with 0.5 g·dm^{-3} UDD concentration in electrolyte are in (1 *c*, *d*). The measured maps of potential distribution for the reference surface are shown in (2 *a*, *b*) and for the nanocomposite are in (2 *c*, *d*). The corresponding topographical images measured for the nickel coating are in (3 *a*, *b*) and for the nanocomposite are in (3 *c*, *d*).

3.2 Corrosion resistance of nickel and nickel-UDD coatings

Potentiodynamic polarization curves of Ni and Ni-UDD coatings obtained in 0.5 M NaCl solution are shown in Fig. 9. The electrochemical corrosion parameters, calculated from the analysis of the polarization curves, are given in Table 7. As can be seen from the presented data, UDD had a notable effect on corrosion properties of the coatings under study. Polarization curves of Ni-UDD coatings obtained from the electrolyte containing 10^{-3} g·dm^{-3} UDD were similar to those of pure Ni coatings, however, a repeatable difference of the cathodic branch of the polarization curve was observed. This can be due to the introduction of the UDD second phase, which is cathodic on its nature relative to Ni. Nevertheless, corrosion potential and current density of these samples were quite similar. Further increase in the UDD concentration to 10^{-2} g·dm^{-3} resulted in a noticeable shift (ca. −0.135 mV) of the corrosion potential to the anodic region, indicating higher corrosion resistance of the surface and corrosion current density in this case decreased ca. 5.5 times as compared to UDD-free coating. Coatings obtained in the electrolyte containing $5 \cdot 10^{-3}$ g·dm^{-3} UDD showed higher corrosion potential but also higher

* Corresponding author
E-mail: Iryna.Makarava@lut.fi

corrosion current density, most probably due to the changes in the microstructure of the electrode surface.

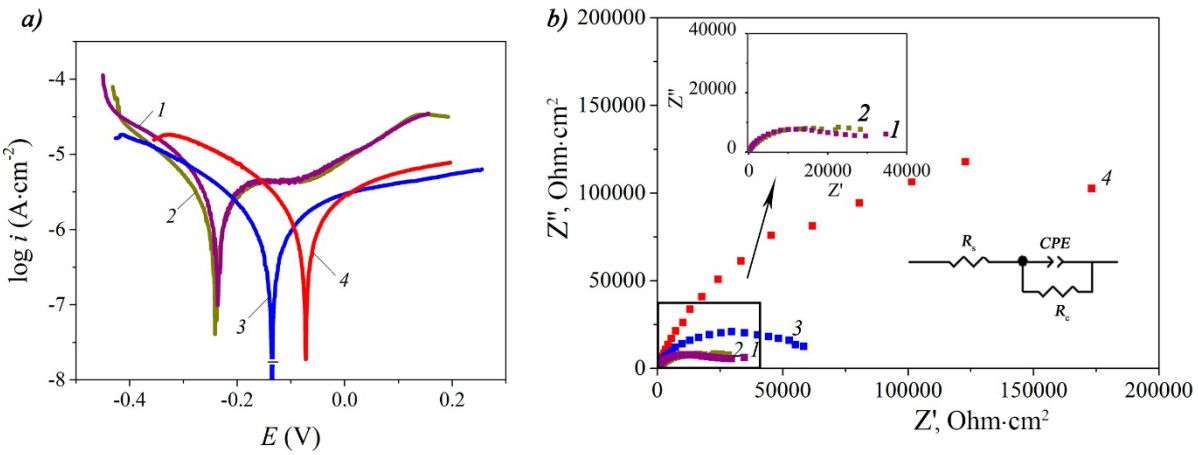

Concentration of UDD in electrolyte, g·dm^{-3}: 1 – 0; 2 – 10^{-3}; 3 – 10^{-2}; 4 – $5\cdot10^{-2}$

Fig. 9. Potentiodynamic polarization curves of Ni and Ni-UDD coatings in 0.5 M NaCl (*a*) Nyquist EIS plots in 0.5 M NaCl solution. Equivalent circuit, used for data analyzes is shown in (*b*) and the zoomed-in area is shown as an inset.

Table 7. Electrochemical parameters extracted from the potentiodynamic polarization curves

Concentration of UDD in electrolyte, g·dm^{-3}	a_a, V	b_a·dec, V	a_c, V	$\|b_c\|$·dec, V	i_{corr}, μA·cm^{-2}	E_{corr}, V
0	0.0388	0.0073	−0.0326	0.4491	0.41	−0.241
10^{-3}	0.0290	0.0505	−0.0235	0.3875	0.38	−0.235
10^{-2}	0.0263	0.0489	−0.0148	0.2442	0.07	−0.135
$5\cdot10^{-2}$	0.0227	0.0848	−0.0245	0.2393	0.14	−0.073

Nyquist plots of bare nickel and nickel-UDD composite coatings are presented in Fig. 9. Obtained spectra presented one capacitive time constant in the form of semi-circle. The impedance spectra were analyzed using equivalent circuit including R_c as charge transfer resistance, CPE element as capacitance of the electrical double layer, and R_s as the solution resistance.

Table 8. Parameters obtained from the fitting of the experiment impedance spectra after exposure to 0.5 M NaCl

* Corresponding author
E-mail: Iryna.Makarava@lut.fi

	Concentration of UDD in electrolyte, $g \cdot dm^{-3}$			
	0	10^{-3}	10^{-2}	$5 \cdot 10^{-2}$
R_s, $\Omega \cdot cm^2$	20.89	18.43	17.82	23.55
Y_1, $S^n/(\Omega \cdot cm^2)$	$4.82 \cdot 10^{-5}$	$6.61 \cdot 10^{-5}$	$3.06 \cdot 10^{-5}$	$3.20 \cdot 10^{-5}$
n	0.87	0.71	0.82	0.84
R_c, $k\Omega \cdot cm^2$	22.36	27.76	58.57	283.99

The EIS results obtained in 0.5 M NaCl show an increase in the charge transfer resistance that indicates improving of corrosion resistance of the CEC compared with the bare nickel coating. The highest R_c value (283.99 $k\Omega cm^2$) was obtained for the coating obtained when the UDD content in the electrolyte was 0.05 $g \cdot dm^{-3}$. Quasicapacitive parameter (Y_1) does not change much with the impedance increase. This indicates an alteration of the relaxation time. The impedance spectroscopy data are consistent with the corrosion currents calculated according to the polarization curves.

Several factors can explain the increase of the corrosion resistance. It is obvious that addition of the UDDs plays a major role in the improved corrosion resistance and they act as an inert physical barrier to the initiation and development of the corrosion attack. In addition, there is a possibility of a large number of microcells formation in the nickel matrix. The UDDs will act as a cathode, and nickel as an anode [4]. Such corrosive galvanic couples contribute to anodic polarization. Thus, Ni-UDD coatings have better corrosion resistance [4].

The key role in another explanation belongs to the texture changing of the coating. It is well known that dense and packed crystal growth planes often dissolve faster due to lower energy required for bond breaking and, therefore, active dissolution of atoms occurs in a certain direction [4]. In this work, the (111) planes were more closely packed compared to the (200) planes and probably contributed to an increase in the corrosion resistance of the studied CEC.

4. Conclusions

The electrochemical stage is the limiting stage of nickel ion reduction in the presence of UDD in the potential ranged from –0.4 to –0.8 V. The UDD addition into the Ni plating electrolyte led to an increase in the cathode polarization and accelerated the transition of nickel to a passive state. The presence of individual ultrafine nanodiamonds was possibly indicated by the ImEFM measurements. The addition of UDDs allowed to obtain a fine crystalline nanocomposite coating with rougher surface topology and smaller crystalline sizes than in case of pure nickel. The deposited UDD-containing coatings demonstrated improved surface microhardness and higher wear resistance with lowered friction coefficients. These coatings

* Corresponding author
E-mail: Iryna.Makarava@lut.fi

demonstrated better corrosion resistance with a clear decrease in corrosion currents and a shift of the corrosion potential to more noble values. The charge transfer resistance (R_c) increased with the addition of UDDs, which is an indicator of the increased corrosion resistance. The increase of UDDs concentration from 10^{-3} to $5 \cdot 10^{-2}$ led to an improved corrosion resistance and lower sliding friction.

5. Acknowledgements

This study was financially supported by the Goverment Research Programme of Belarus (No. 20141326).

References

[1]. L. Wang, Effects of nano-diamond particles on the structure and tribological property of Ni-matrix nanocomposite coatings / L. Wang, Y. Gao, Q. Xue, H. Liu, T. Xu // Materials Science and Engineering A, 2005, 390. − P. 313-318

[2]. K. Strzelczak, Quality control of a metallic dental bur with a diamond coating / Katarzyna Strzelczak // Production engineering archives. 19. 2018. P. 26-29. https://doi.org/10.30657/pea.2018.19.06.

[3] M. Adabi, A.A. Amadeh. Electrodeposition mechanism of Ni−Al composite coating, Trans. Nonferrous Met. Soc. China 24 (2014) 3189−3195. https://doi.org/10.1016/S1003-6326(14)63459-2.

[4] A. Hefnawy, N. Elkhoshkhany, A. Essam. Ni–TiN and Ni-Co-TiN composite coatings for corrosion protection: Fabrication and electrochemical characterization, J. Alloys Compd. 735 (2018) 600−606. https://doi.org/10.1016/j.jallcom.2017.11.169.

[5] S.-K. Kim, T.-S. Oh. Electrodeposition behavior and characteristics of Ni-carbon nanotube composite coatings, Trans. Nonferrous Met. Soc. 21 (2011) s.68−s.72. https://doi.org/10.1016/S1003-6326(11)61063-7.

[6] B. Pandeya, D. Das, A.K. Kar. Electrical and magnetic properties of electrodeposited nickel incorporated diamond-like carbon thin films, Appl. Surf. Sci. 337 (2015) 195–207. https://doi.org/10.1016/j.apsusc.2015.02.092.

[7] C. Wang, L. Shen, M. Qiu, Z. Tian, W. Jiang. Characterizations of Ni-CeO_2 nanocomposite coating by interlaced jet electrodeposition, J. Alloys Compd. 727 (2017) 269−277. https://doi.org/10.1016/j.jallcom.2017.08.105.

[8]. S. Ahmadiyeh, A. Rasooli, M.G. Hossein. Ni–B/SiC nanocomposite coating obtained by pulse plating and evaluation of its electrochemistry and mechanical properties, Surface Engineering https://doi.org/10.1080/02670844.2018.1498823.

* Corresponding author
E-mail: Iryna.Makarava@lut.fi

[9] C. Liu, F. Su, J. Liang. Producing cobalt–graphene composite coating by pulse electrodeposition with excellent wear and corrosion resistance, Appl. Surf. Sci. 351 (2015) 889−896. https://doi.org/10.1016/j.apsusc.2015.06.018.

[10] M.Y. Rekha, S. Chandan. Microstructure and corrosion properties of zinc-graphene oxide composite coatings. Corrosion Science. Vol. 152, 15 2019, P. 234−248. https://doi.org/10.1016/j.corsci.2019.03.015.

[11] C.T.J. Low, R.G.A. Wills, F.C. Walsh. Electrodeposition of composite coatings containing nanoparticles in a metal deposit, Surf. Coat. Technol. 201 (2006) 371–383. https://doi.org/10.1016/j.surfcoat.2005.11.123.

[12] V.V. Yaskelchik. Sedimentation of ultradispesed diamonds in citrate electrolyte for electrodeposition of copper / Yaskelchik V.V., Anan'ev M.V., Ostanina T.N., Zharsky I.M., Chernik A.A., Ostanin N.I. // Izvestiya visshih uchebnih zavedenii. Poroshkovaya metallurgiya i funkcionalnie pokritiya. 2017 (4). P. 53−61. https://doi.org/10.17073/1997-308X-2017-4-53-61.

[13] M. Sheng, W. Weng, Y. Wang, Q. Wu, S. Hou. Co-W/CeO_2 composite coatings for highly active electrocatalysis of hydrogen evolution reaction, J. Alloys Compd. 743 (2018) 682−690. https://doi.org/10.1016/j.jallcom.2018.01.356.

[14] N. Elkhoshkhany, A. Hafnway, A. Khaled. Electrodeposition and corrosion behavior of nano-structured Ni-WC and Ni-CoWC composite coating, J. Alloys Compd. 695 (2017) 1505−1514. https://doi.org/10.1016/j.jallcom.2016.10.290.

[15] A. Laszczynska, J. Winiarski, B. Szczygieł, I. Szczygieł. Electrodeposition and characterization of Ni–Mo–ZrO_2 composite coatings, Appl. Surf. Sci. 369 (2016) 224−231. https://doi.org/10.1016/j.apsusc.2016.02.086.

[16] A.A. Kasach, I.I. Kurilo, D.S. Kharitonov, S.L. Radchenko, I.M. Zharskii. Effect of Sonochemical Treatment Modes on the Electrodeposition of Cu–Sn Alloy from Oxalic Acid Electrolyte, Russian Journal of Applied Chemistry, (2018) 91 (4) P. 591−596 doi: 10.1134/S1070427218040092.

[17] F. Wang, S. Arai, M. Endo. Preparation of nickel-carbon nanofiber composites by a pulse-reverse electrodeposition process, Electrochem. Commun. 7 (2005) 674−678. https://doi.org/10.1016/j.elecom.2005.04.016.

[18] B.-G. An, L.-X. Li, H.-X. Li, Electrodeposition in the Ni-plating bath containing multi-walled carbon nanotubes, Mater. Chem. Phys. 110 (2008) 481−485. https://doi.org/10.1016/j.matchemphys.2008.03.007.

[19] I.V. Antihovich, N.M. Ablazhey, A.A. Chernik, I.M. Zharsky. Electrodeposition of Nickel and Composite Nickel-Fullerenol Coatings from Low-Temperature Sulphate-Chloride-

* Corresponding author
E-mail: Iryna.Makarava@lut.fi

Isobutyrate Electrolyte, Procedia Chemistry. 10 (2014) 373–377. https://doi.org/10.1016/j.proche.2014.10.063.

[20] D. Liua, W. Zhao, S. Liu, Q. Cen, Q. Xue. Comparative tribological and corrosion resistance properties of epoxy composite coatings reinforced with functionalized fullerene C_{60} and graphene Surface and Coatings Technology, Vol. 286, 25 2016, P. 354−364.

[21]. G. Sheela, M. Pushpavanam. Diamond-dispersed electroless nickel coatings, Metal Finishing, Vol. 100, Iss. 1, 2002, P. 45−47. https://doi.org/10.1016/S0026-0576(02)80018-6.

[22]. M. Wang, R.-C. Wang, C. Peng, Y. Feng, C. Zhang, L. Deng. Preparation of Ni-diamond composite coating by composite electroplating /Journal of Central South University (Science and Technology), 2013 44 (7) : P. 2688−2695.

[23]. H. Ogihara, A. Hara, K. Miyamoto, N. K. Shrestha, T. Kaneda, S. Ito, T. Saji. Synthesis of super hard Ni–B/diamond composite coatings by wet processes / Chem. Commun., 2010,46, 442−444. https://doi.org/10.1039/B914242H

[24]. T. Tsubota. Composite electroplating of Ni and surface-modified diamond particles with silane coupling regent / T. Tsubota, Sh. Tanii, T. Ishida, M. Nagata, Y. Matsumoto // Diamond and Related Materials, 2005, 14. − P. 608-612. https://doi.org/10.1016/j.diamond.2005.01.013.

[25]. I.V. Antsikhovich. Properties of composite nickel coatings obtained from low-temperature tartaric electrolytes / I.V. Antsikhovich, A.A. Chernik, I.M. Zharsky // Galvanotechnika I obrabotka poverhnosti. – 2015. – Vol. 23. – № 2. – P. 38–43. https://doi.org/10.1016/j.proche.2014.10.063.

[26]. G.K. Burkat. Preparation of composite electrochemical nickel-diamond and iron-diamond coatings in the presence of detonation synthesis nanodiamonds / G.K. Burkat, T. Fujimura, V.Yu. Dolmatov, E.A. Orlova, M.V. Veretennikova // Diamond and Related Materials, 2005, 14. − P. 1761−1764. https://doi.org/10.1016/j.diamond.2005.08.004.

[27]. L. Wang. Effects of nano-diamond particles on the structure and tribological property of Ni-matrix nanocomposite coatings / Liping Wang, Yan Gao, Qunji Xue, Huiwen Liu, Tao Xu // Materials Science and Engineering A, 2005, 390. − P. 313−318. https://doi.org/10.1016/j.msea.2004.08.033.

[28]. L. Wang. Effects of bivalent Co ion the co-deposition of nickel and nano-diamond particles / Liping Wang, Yan Gao, Huiwen Liu, Qunji Xue, Tao Xu // Surf. Coat. Technol., 2005, 191. − P. 1−6. https://doi.org/10.1016/j.surfcoat.2004.03.047.

[29]. S. You. Probing structural stability of double-walled carbon nanotubes at high non-hydrostatic pressure by Raman spectroscopy / Sh. You, M. Mases, I. Dobryden, A.A. Green, M.C. Hersam, A.V. Soldatov // High Pressure Research. V. 31, No. 1, 2011. P. 186–190. https://doi.org/10.1080/08957959.2011.562897.

* Corresponding author
E-mail: Iryna.Makarava@lut.fi

[30] T. Xu, K. Xu, J. Zhao. TEM and HREM studies on ultradispersed diamonds containing soot formed by explosive detonation, Materials Science and Engineering: B, Vol.38, Iss. 1–2, 1996, P. L1-L4. https://doi.org/10.1016/0921-5107(95)01526-4.

[31] V. Yu. Dolmatov Detonation synthesis ultradispersed diamonds: Properties and applications 2001 Russian Chemical Reviews 70 (7) : 607−626. https://doi.org/10.1070/RC2001v070n07ABEH000665.

[32] L. Jinlong, L. Tonxiang, W. Chen. Effect of electrodeposition temperature on grain orientation and corrosion resistance of nanocrystalline pure nickel, J. Solid State Chem. 240 (2016) 109–114. https://doi.org/10.1016/j.jssc.2016.05.025.

[33] F. Nasirpouri, M.R. Sanaeian, A.S. Samardak, E.V. Sukovatitsina, A.V. Ognev, L.A. Chebotkevich, M.-G. Hosseini, M. Abdolmaleki. An investigation on the effect of surface morphology and crystalline texture on corrosion behavior, structural and magnetic properties of electrodeposited nanocrystalline nickel films, Appl. Surf. Sci. 276 (2013) 604–608. https://doi.org/10.1016/j.apsusc.2013.12.053.

[34] N.P. Wasekar, P. Haridoss, S.K. Seshadri, G. Sundararajan. Influence of mode of electrodeposition, current density and saccharin on the microstructure and hardness of electrodeposited nanocrystalline nickel coatings, Surf. Coat. Technol. 291 (2016) 130–140. https://doi.org/10.1016/j.surfcoat.2016.02.024.

[35] H. Alimadadi, A.B. Fanta, T. Kasama, M.A.J. Somers, K. Pantleon. Texture and microstructure evolution in nickel electrodeposited from an additive-free Watts electrolyte, Surf. Coat. Technol. 299 (2016) 1−6. https://doi.org/10.1016/j.surfcoat.2016.04.068.

[36] B. Lv, Z. Hu, X. Wang, B. Xu. Electrodeposition of nanocrystalline nickel assisted by flexible friction from an additive-free Watts bath, Surf. Coat. Technol. 270 (2015) 123–131. https://doi.org/10.1016/j.surfcoat.2015.03.012.

[37] I.V. Makarova, D.S. Kharitonov, I.B. Dobryden, A.A. Chernik. Corrosion behavior in acid and alkaline media of nickel coatings deposited at room temperature, Russ. J. Appl. Chem. 91 (2018) 1441–1450. https://doi.org/ 10.1134/S1070427218090069.

[38] I.V. Antsikhovich, D.S. Kharitonov, A.A. Chernik, I.B. Dobryden. Corrosion resistance of nickel coatings deposited from low-temperature nickel-plating electrolytes, Russ. J. Appl. Chem. 90 (2017) 566–573. https://doi.org/10.1134/S1070427217040127.

[39] D. Platz, E.A. Tholén, D. Pesen, D.B. Haviland. Intermodulation atomic force microscopy Appl. Phys. Lett. 92, 153106 (2008); https://doi.org/10.1063/1.2909569

[40] R. Borgani, D. Forchheimer, J. Bergqvist, P.-A. Thorén, O. Inganäs, D.B. Haviland. Intermodulation electrostatic force microscopy for imaging surface photo-voltage, Appl. Phys. Lett. 105, 143113 (2014); https://doi.org/10.1063/1.4897966

* Corresponding author
E-mail: Iryna.Makarava@lut.fi

[41] S. Mrowec, Z. Grzesik. Oxidation of nickel and transport properties of nickel oxide / Journal of Physics and Chemistry of Solids 65 (2004) 1651–1657. https://doi.org/10.1016/j.jpcs.2004.03.011.

[42] M.A.M. Ibrahim, R.M. Al Radadi. Role of glycine as a complexing agent in nickel electrodeposition from acidic sulphate bath Int. J. Electrochem. Sci., 10 (2015) 4946 – 4971

[43] T.D. Khokhlova, G.R. Yunusova, S.N. Lanin. Adsorption of Dyes in Studying the Surface Chemistry of Ultradispersed Diamond Russian Journal of Physical Chemistry A, 2018, Vol. 92, No. 5, pp. 1006–1010. https://doi.org/10.1134/S0036024418050175.

[44] Y.H. Ahmad, J. Tientong, M. Nar, N. D'Souza, A.M.A. Mohamed, T.D. Golden. Characterization and corrosion resistance of electrodeposited Ni–Mo–silicate platelet nanocomposite coatings, Surf. Coat. Technol. 259 (2014) 517–525. http://dx.doi.org/10.1016/j.surfcoat.2014.10.036.

* Corresponding author
E-mail: Iryna.Makarava@lut.fi

Highlights

1. Ni-nanodiamond coatings were electrodeposited from nickel-plating electrolyte at ambient temperature.

2. The composite coatings had a higher hardness, a higher wear resistance and roughness, lower friction coefficient than pure nickel coatings.

3. Nanodiamonds improved the corrosion resistance of composite coating.

* Corresponding author
E-mail: Iryna.Makarava@lut.fi

Supplementary

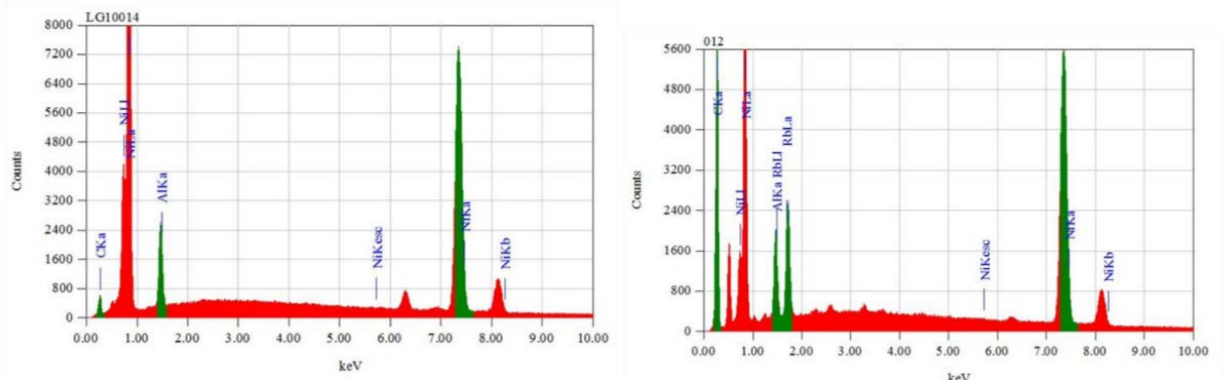

(*a*) (*b*)

Fig 1S. EDS plots of nickel (*a*) and nickel-UDD (*b*) coatings

* Corresponding author
E-mail: Iryna.Makarava@lut.fi